Experimental study of resonant states in ^{27}P via elastic scattering of ^{26}Si+p

H. S. Jung, C. S. Lee,* Y. K. Kwon,† J. Y. Moon, J. H. Lee, and C. C. Yun†
Department of Physics, Chung-Ang University, Seoul 156-756, Republic of Korea

S. Kubono, H. Yamaguchi, T. Hashimoto, D. Kahl, and S. Hayakawa
Center for Nuclear Study (CNS), University of Tokyo, RIKEN Campus, 2-1 Hirosawa, Wako, Saitama 351-0198, Japan

Seonho Choi, M. J. Kim, and Y. H. Kim
Department of Physics and Astronomy, Seoul National University, Seoul 151-742, Republic of Korea

Y. K. Kim
Department of Nuclear Engineering, Hanyang University, Seoul 133-791, Republic of Korea and
Institute for Basic Science, Daejeon 305-811, Republic of Korea

J. S. Park
Department of Nuclear Engineering, Hanyang University, Seoul 133-791, Republic of Korea

E. J. Kim
Division of Science Education, Chonbuk National University, Jeonju 561-756, Republic of Korea

C.-B. Moon
Faculty of Sciences, Hoseo University, Asan 336-795, Republic of Korea

T. Teranishi
Department of Physics, Kyushu University, 6-10-1 Hakozaki, Fukuoka 812-8581, Japan

Y. Wakabayashi
Advanced Science Research Center, JAEA, Tokai, Ibaraki 319-1195, Japan

N. Iwasa and T. Yamada
Department of Physics, Tohoku University, Aoba, Sendai, Miyagi 980-8578, Japan

Y. Togano
RIKEN Nishina Center, 2-1 Hirosawa, Wako, Saitama 351-0198, Japan

S. Kato
Department of Physics, Yamagata University, 1-4-12 Kojirakawa-machi, Yamagata 990-8560, Japan

S. Cherubini and G. G. Rapisarda
Laboratori Nazionali del Sud-INFN, Catania, Italy and
Dipartimento di Fisica e Astronomia, Università di Catania, Catania, Italy

(Received 10 February 2012; revised manuscript received 16 March 2012; published 3 April 2012)

Proton resonant states in ^{27}P were studied by the resonant elastic scattering of $^{26}\mathrm{Si}+p$ with a ^{26}Si radioactive ion beam bombarding a thick H_2 gas target with the inverse kinematics method. The properties of these resonance states are important to better constrain the production rates of the $^{26}\mathrm{Si}(p,\gamma)^{27}\mathrm{P}$ reaction. This is one of the astrophysically important reactions needed to understand proton-rich nucleosynthesis such as the galactic production of ^{26}Al and energy generation in explosive stellar environments. Although there are recent studies on the resonant structure in ^{27}P, large uncertainties remain, and only a few levels are known. In this work, resonant states were observed over the excitation energies range of 2.3 to 3.8 MeV with high statistics and without background contamination within the target. The resonance parameters were extracted by an R-matrix analysis of the excitation function. The $^{26}\mathrm{Si}(p,\gamma)^{27}\mathrm{P}$ stellar reaction rate has been evaluated, including high-lying resonances found in this work.

DOI: 10.1103/PhysRevC.85.045802 PACS number(s): 25.40.Ny, 23.20.Lv, 26.30.−k, 27.30.+t

I. INTRODUCTION

The rapid proton capture process (rp process) is a dominant reaction sequence in high-temperature hydrogen burning. In explosive stellar environments like novae or x-ray bursts, processing occurs mostly via the rp process, a sequence of (p,γ) reactions, (α,p) reactions, and β decays that is responsible for the burning of hydrogen into heavier elements, especially proton-rich nuclides with the mass number up to $A \sim 100$ [1–3]. Therefore, accurate reaction rates for nuclear reactions on the rp process are essential for an understanding of the nucleosynthesis processes and energy production in hot stellar hydrogen burning. The direct measurement cross section for proton capture reactions by proton-rich nuclei requires a radioactive target with high density or a radioactive ion beam (RI beam) with high intensity because of the increasing Coulomb barrier. For that reason, many of the nuclear data relevant to the rp process are the result of indirect nuclear spectroscopy. As is known, in the case of low level densities in the compound nucleus, the reaction rates are determined by the contributions of isolated narrow resonances as well as by tail contributions of high-lying broad resonances and by nonresonant direct capture within the astrophysically relevant energy window. The resonant states can be investigated by proton elastic scattering, which is very useful to study proton resonances in proton-rich unstable nuclei [4–6]. Through the measurement of resonant elastic scattering, the resonance parameters such as excitation energies, spin parities, and proton partial widths for resonance states can be obtained, which can then be used to calculate the stellar thermonuclear reaction rate. In this paper, we report the experimental results for elastic resonant scattering of $^{26}\mathrm{Si}+p$ using an RI beam of ^{26}Si to investigate the $^{26}\mathrm{Si}(p,\gamma)^{27}\mathrm{P}$ reaction. This reaction is one of the important ones in the rp-process path for understanding the nucleosynthesis in explosive hydrogen burning [7,8].

The $^{26}\mathrm{Si}(p,\gamma)^{27}\mathrm{P}$ reaction is also relevant to the production of ^{26}Al, which is the first cosmic radioactivity ever detected and is a piece of evidence implying that galactic nucleosynthesis is an ongoing process [9,10]. Although various possible sites like massive stars, novae, and supernovae are suggested for the production of ^{26}Al [11,12], specific knowledge of its origin is not yet clear due to a large uncertainty in its production. The ground state of ^{26}Al ($^{26}\mathrm{Al}^{gs}$, $t_{1/2} = 0.717$ milion years) β decays to the first excited state in ^{26}Mg, giving rise to a 1.809-MeV γ ray via the electromagnetic de-excitation. Besides, the first excited state of ^{26}Al ($^{26}\mathrm{Al}^{m}$, $t_{1/2} = 6.34$ s) β decays to the ground state of ^{26}Mg, which does not result in the emission of a γ ray. In principle, internal transitions (γ decay) from the isomer to the ground state are inhibited by their large nuclear spin difference ($\Delta I = 5$). However, if the $^{26}\mathrm{Al}^{m}$ is effectively connected with the $^{26}\mathrm{Al}^{\mathrm{gs}}$ through the thermal population of excited levels, then this thermal process would enhance the production of $^{26}\mathrm{Al}^{\mathrm{gs}}$. The critical temperature above which that thermal equilibrium takes place is evaluated to be 0.4 GK [13–15]. The $^{26}\mathrm{Si}(p,\gamma)^{27}\mathrm{P}$ reaction competes with the β decay of ^{26}Si to $^{26}\mathrm{Al}^{m}$, which can produce $^{26}\mathrm{Al}^{\mathrm{gs}}$ via thermal excitation; therefore the destruction of ^{26}Si by proton capture is important and the rate of this reaction should be determined accurately for an estimation of the production of $^{26}\mathrm{Al}^{\mathrm{gs}}$ at higher temperatures in explosive hydrogen burning [16,17].

The structure of ^{27}P has been studied with measurements of the $^{32}\mathrm{S}(^{3}\mathrm{He},^{8}\mathrm{Li})^{27}\mathrm{P}$ [18], $^{28}\mathrm{Si}(^{7}\mathrm{Li},^{8}\mathrm{He})^{27}\mathrm{P}$ [19], and Coulomb dissociation of ^{27}P [20]. Three resonant states above the proton threshold were observed at low-lying energies, and two states above $E_x \sim 3.1$ MeV were found. However, the knowledge of the structure of this nucleus is still insufficient because of uncertain resonance parameters, such as resonance energies and spin-parity assignments. Consequently, there is the possibility of finding a number of experimentally unobserved states in ^{27}P suggested by a comparison with its mirror nucleus ^{27}Mg [21] and shell-model calculations. In addition, the stellar network calculations done by Runkle *et al.* [15], Guo *et al.* [16], and Timofeyuk *etal.* [17] had uncertainties in their results because only limited information concerning ^{27}P was used as an input, which was adopted from Refs. [19,22]. The evaluation of the total thermonuclear reaction rates for $^{26}\mathrm{Si}(p,\gamma)^{27}\mathrm{P}$ by Iliadis *et al.* [23] was also based on very limited experimental data.

In the present study, we measured the excitation function over the energy range of 2.3–3.8 MeV in ^{27}P. The excited states of ^{27}P in this energy region have previously been measured by the $^{1}\mathrm{H}(^{26}\mathrm{Si},p)^{26}\mathrm{Si}$ reaction [24,25]; however, several candidates for the resonant states were expected but were not confirmed because of poor statistics and background contaminations originating from the beam's interaction with carbon atoms contained in the CH_2 target. The goal of this experiment was to search for high-lying states in ^{27}P by proton-elastic resonant scattering in a broad range within the Gamow window above the proton threshold with a thick-hydrogen gas target, free from any background contribution in the target, and high statistics using inverse kinematics.

II. EXPERIMENTAL PROCEDURE

The measurement of the $^{26}\mathrm{Si}+p$ elastic scattering was performed at the low-energy RI beam facility of the Center for Nuclear Study (CNS), CRIB (CNS radioactive ion beam separator), located at the University of Tokyo [26,27], by bombarding a ^{26}Si radioactive ion beam onto a H_2 gas target in inverse kinematics [28] and detecting scattered protons using silicon detectors for a ΔE-E telescope. We applied the thick-target method [29,30] to scan the entire energy region of interest simultaneously. The excitation function was obtained from the scattered proton energy spectrum by a kinematics conversion process. The experimental setup is shown in Fig. 1.

A ^{24}Mg primary beam with an energy of 7.5 MeV/A and an intensity of 1.6 eμA extracted from the AVF cyclotron bombarded a ^{3}He gas target at 550 Torr and 90 K [31]. Then a secondary beam of ^{26}Si was produced by the $^{3}\mathrm{He}(^{24}\mathrm{Mg},^{26}\mathrm{Si})n$ reaction and was separated by CRIB using the in-flight method. The ^{26}Si beam had a well-defined energy of 132.8 ± 0.6 MeV.

*cslee@cau.ac.kr
†Present address: Institute for Basic Science, Daejeon 305-811, Republic of Korea.

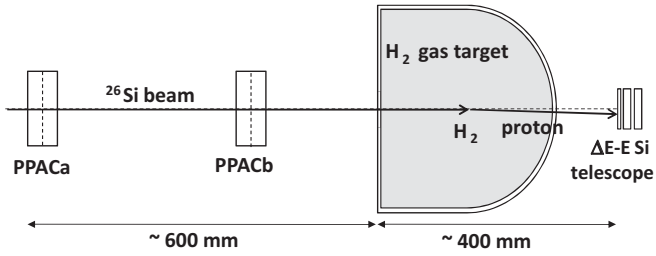

FIG. 1. Experimental setup of the measurement of the $^{26}\mathrm{Si}+p$ elastic scattering in inverse kinematics at the final focal plane.

The beam intensity and purity were up to 1.2×10^4 pps and about 23%, respectively, after passing through a Wien filter, which significantly purifies the secondary beam. Two parallel plate avalanche counters (PPACs) [32] were used to measure the position and timing of the incoming beam with a position resolution of 1 mm or better. The secondary target was a thick hydrogen gas target, which was at 330 Torr, housed in a 300-mm-radius semicylindrical shape, and sealed with a thin (2.5-μm) Havar foil as a beam entrance window and with a thin (25-μm) aluminized Mylar foil as an exit window. The ^{26}Si beam lost energy while continuously passing through the thick target mainly due to collisions with electrons in the hydrogen atoms. Therefore, simultaneous measurements of the cross section of various incident energies can be performed with one incident beam energy. Another main feature is that this target is free from background contributions over the scanned energy region of interest owing to the pure hydrogen gas in comparison with a solid polyethylene (CH_2) target, which can contribute to the background by carbon atoms.

Protons elastically scattered to forward angles in the laboratory frame were detected by a ΔE-E telescope, which consisted of a 75-μm-thick double-sided 16-channel-by-16-channel strip position-sensitive silicon detector (PSD) and two 1.5-mm single-channel silicon strip detectors (SSDs), both with an area of 5×5 cm^2. The telescope was placed at a distance of ~400 mm from the beginning of the target at $\theta_{\mathrm{lab}}=0^\circ$. Since the energy of the recoil protons was high enough to punch through the PSD (ΔE) but stopped in the first SSD (E), high-energy protons originating upstream of the scattering chamber could be eliminated by vetoing events from the second SSD. Proton events were selected by using the energy measured from the ΔE-E detector and timing information between the PPAC and the SSD. The energy calibration for the silicon detectors was performed separately with α sources, and further calibration was carried out altogether (ΔE-E) by using the secondary proton beams separated by their magnetic rigidity at several energy points, $E_p=4$, 5, 6, 7, 8, 9, 10, 11, and 12 MeV. The measurement of proton elastic scattering was successfully performed over 74 h, and we obtained high statistics for the $^{26}\mathrm{Si}+p$ measurement.

III. RESULTS AND DATA ANALYSIS

A. Experimental results

By calculating the kinematics, including energy loss in the target, the measured proton energy of each event was converted

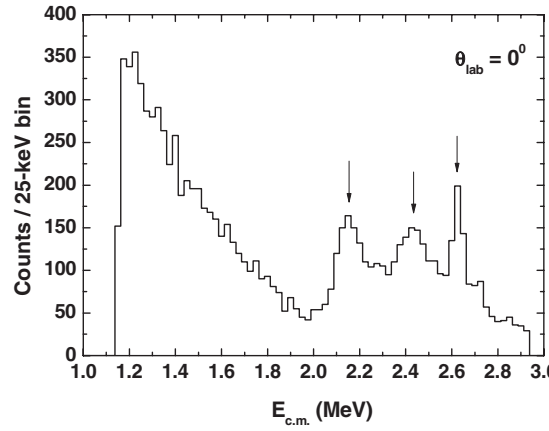

FIG. 2. Energy spectrum of proton for $^{26}\mathrm{Si}+p$ elastic scattering after conversion to the center-of-mass frame at $\theta_{\mathrm{lab}}=0^\circ$. Arrows indicate the prominent resonance states.

to a center-of-mass energy for the $^{26}\mathrm{Si}+p$ system ($E_{\mathrm{c.m.}}$) by

$$E_{\mathrm{c.m.}}=\frac{M_{\mathrm{Si}}+M_p}{4M_{\mathrm{Si}}\cos^2\theta_{\mathrm{lab}}}E_p, \tag{1}$$

where M_{Si} and M_p are the nuclear masses of the heavy ^{26}Si beam particle and the scattered proton, respectively, E_p is the measured energy of the scattered protons in the laboratory frame, and θ_{lab} is the scattering angle between the proton's scattering direction and the beam direction.

Figure 2 shows the proton spectrum for $^{26}\mathrm{Si}+p$ elastic scattering in the center-of-mass frame after complete conversion. Three prominent resonance peaks can be clearly seen in the region of 2.1–2.6 MeV, and positions and widths of these peaks are essentially in good agreement with the previous result [25]. The low-energy region below ~2 MeV contains contributions mainly from Coulomb scattering. The energy loss calculation using the SRIM code [33], which was used for the kinematics conversion process, appears to be quite reliable. The upper limit of $E_{\mathrm{c.m.}}$ from the measured data is about 2.9 MeV as seen in Fig. 2, which is in good accord with $E_{\mathrm{c.m.}}$ expected from the beam energy at the beginning of the target. The experimental differential cross sections of the proton scattering events were calculated from the number of selected proton events and incident beam ions, the target thickness, and the different solid angles, depending on the interaction position in the thick target. Corresponding excitation energies in ^{27}P were calculated through the relation that $E_{\mathrm{x}}=E_{\mathrm{c.m.}}+0.859$ (MeV) [18]. The overall uncertainty (1σ with of a Gaussian distribution) in $E_{\mathrm{c.m.}}$ of the excitation function was estimated to be 27–33 keV, depending on the energy. The energy straggling of the ^{26}Si beam and the protons passing through the target and windows was calculated by the program LISE++ [34] with an 1σ. The energy resolution of the ΔE-E detector was obtained by fit with a Gaussian function, and angular uncertainty due to the finite size of the detector and the distance depending on the target thickness was calculated using the geometrical relation. Finally, the overall uncertainty was analyzed by an error propagation.

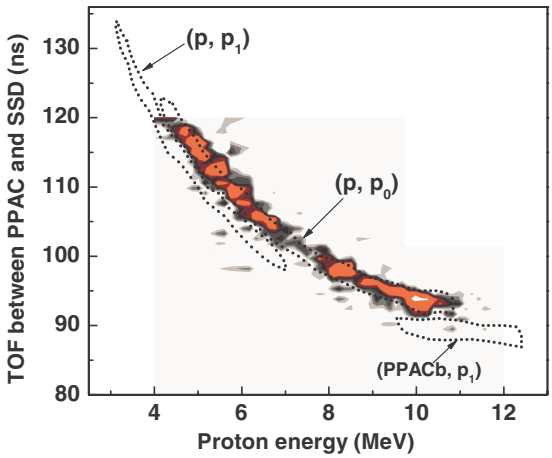

FIG. 3. (Color online) Two-dimensional plot of TOF between the PPAC and SSD vs proton total energy as calculated (dotted curves) and experimental results for identification of elastic and inelastic scattering events. We performed the calculation with the time resolution of the detection system being about 4 ns.

Since the proton spectrum was obtained under the assumption of kinematics describing only the elastic scattering of $^{26}\mathrm{Si}+p$, the resonant elastic and inelastic scattering events have to be clearly separated. A two-dimensional plot of the time of flight (TOF) between the first PPAC and the SSD versus the proton energy was used to deduce the type of proton scattering (elastic vs inelastic). The beam travels slower than recoiling protons within the target, and due to the target's elongated nature, protons have different flight times depending on the position in the target and type of scattering. This enables elastic scattering events to be separated from the background sources such as the excited states of ^{26}Si, the exit window of the target, the PPACs (these contain hydrogen), and other upstream sources. The required time separation to distinguish events which are the transition to the ground and the first excited state was about 4 ns, according to the estimation for our target with a length of 300 mm. Since the time resolution (in full width at half maximum, FWHM) obtained for the SSD detector was about 2.2 ns in this work, it was an easy task to discriminate between elastic and inelastic scattering events. Figure 3 shows the TOF vs energy plot as calculated and experimental results for event identification. In the figure (p, p_0) and (p, p_1) indicate the loci of calculated transitions to the ground state (elastic scattering events) and to the first excited state of ^{26}Si ($E_\mathrm{x}=1.796$ MeV, inelastic scattering events), respectively. (PPACb, p_1) represents the first excited, resonant inelastic scattering in PPACb. Since protons by scattering events from the PPACa and PPACb ground-state transition have higher energy above ~13 MeV, they are not represented in this figure. As shown in Fig. 3, no evident inelastic structure is seen. This means that the reaction should mostly correspond to the ground state of ^{27}P.

B. *R*-matrix analysis on the excitation function

The excitation function of $^{26}\mathrm{Si}+p$ elastic scattering cross sections obtained in this work is shown in Figs. 4 and 5. Structures with several peaks were clearly observed. We performed an analysis using the R-matrix calculation code SAMMY 8.0.0 [35,36] to deduce resonance parameters such as excitation energy E_x, spin J, parity π, and proton partial width Γ_p of resonance states. We chose the channel radius given by $R_c=1.45({A_t}^{1/3}+{A_p}^{1/3})$ fm [25] where A_t and A_p are the mass numbers of the target and projectile, respectively. The fit result was found not to be very sensitive to changes in the channel radius. Many R-matrix fits with all possible spin-parity combinations for observed resonances were attempted. The various spin parities (J^π) of each resonance were fixed while the energy and the proton partial width (Γ_p) were taken as free parameters. Since the decay width of the γ-decay channel (Γ_γ) is much smaller than those of the proton-decay channel in the present work, $\Gamma_\mathrm{tot}=\Gamma_p+\Gamma_\gamma\sim\Gamma_p$. The energy broadening due to the experimental resolution, 27–33 keV (1σ), depending on the energy, was considered in the R-matrix calculations.

Since the spin parity of the proton is $J^\pi=1/2^+$ and that of the ground state of ^{26}Si is 0^+, the incident channel spin is $s=1/2$. Therefore, allowed spin parities of the compound nucleus, ^{27}P, are assigned as $J^{(-1)^l}$, where $J=l\pm1/2$ and l is the relative orbital quantum number of the proton with respect to the nucleus. It can be seen that no negative parity states are observed in the mirror ^{27}Mg nucleus in the present energy region except for the $J^\pi=3/2^-$ state at higher energy, as shown in Fig. 6. Therefore, a resonance found in this energy region most likely has an assignment of positive parity. Among the prominent peaks, the lowest and broadest resonance peak observed around 2.12 MeV was reproduced by the R-matrix calculation with all possible spin parities with inclusion of Coulomb scattering for the low-energy region [Fig. 4(a)]. This resonance was fitted well with a $J^\pi=1/2^+$ assignment. No other assignment ($J^\pi=3/2^+,5/2^+$, or $7/2^+$) could reproduce the high energy part (2.2–2.3 MeV). The result calculated with both $J^\pi=3/2^+$ and $5/2^+$, showing a similar pattern, was not satisfactory for the low-energy tail of experimental data sharply up to the first prominent peak, either. However, since there was still a small discrepancy between the data and the calculated curve obtained with the $J^\pi=1/2^+$ only, we introduced a g-wave resonance of $J^\pi=7/2^+$ at 2.02 MeV to resolve the discrepancy. The fitting result was improved in view of the existence of a small bump at 2.02 MeV and a better-fit height of the first prominent peak [see solid curve in Fig. 4(b)]. Other $J^\pi=3/2^+$ and $5/2^+$ could not satisfy good fits of the peak around 2.12 MeV; on the contrary, fitting results were worse than in the case of $J^\pi=1/2^+$ only. Finally, the best fit was obtained as $J^\pi=7/2^+$ and $1/2^+$ at 2.02 and 2.12 MeV, respectively, in this energy region.

The second prominent peak around 2.48 MeV was considered to be composed of two resonances. We calculated using just one state for this level for comparison as shown in Fig. 4(c). While the black dashed curve shows disagreement with the experimental data (assuming $J^\pi=3/2^+$), fits with other spin-parity assignments ($J^\pi=1/2^+,5/2^+,7/2^+$) totally deviated from the data and were worse than in the case of $J^\pi=3/2^+$. However, assuming an additional resonance in the valley in the middle of the two prominent peaks (around 2.54 MeV) yields

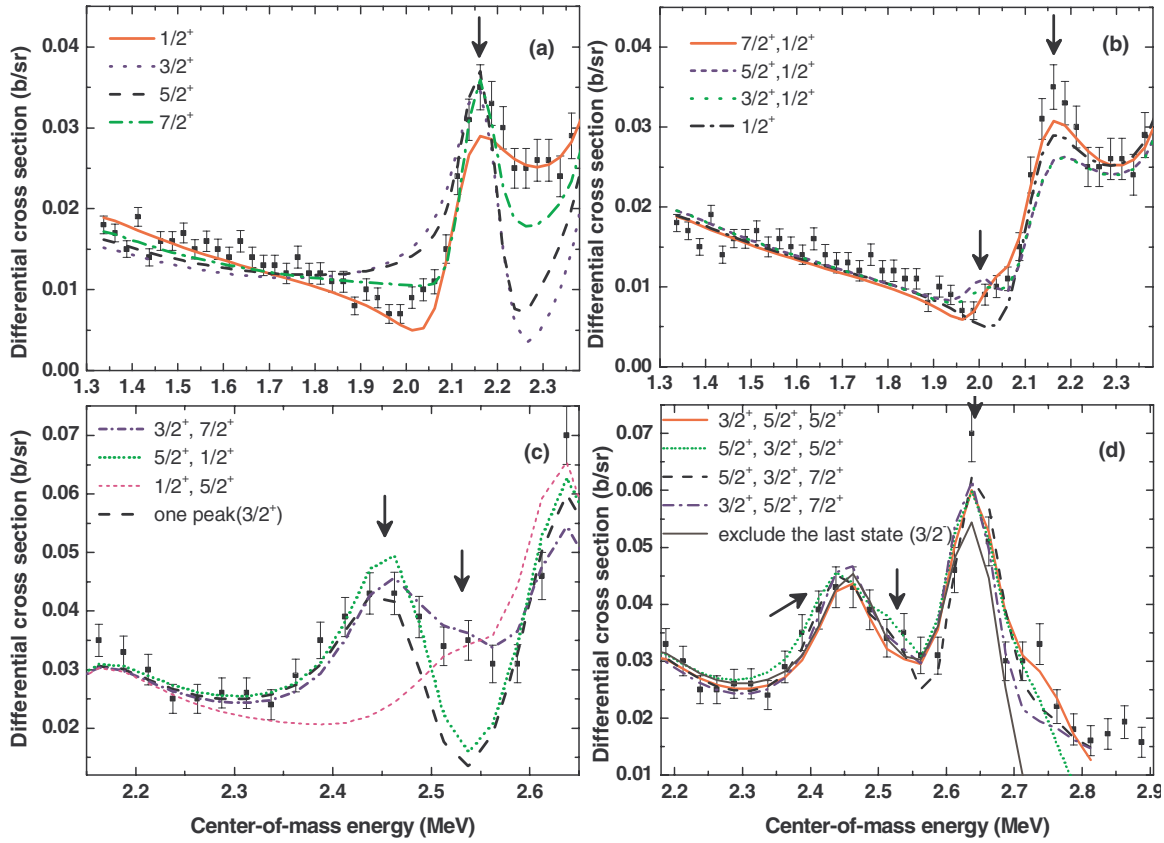

FIG. 4. (Color online) Excitation function for $^{26}\mathrm{Si}+p$ elastic scattering cross section fitted by the R-matrix calculation. (a) Fit for the low-energy region with calculations assuming four candidate spin parities. The best fit is shown in (b) for resonance states at this energy region where a small resonance at 2.02 MeV is included. (c) The doublet for the broad second peak is required to fit around 2.54 MeV by comparison with the black dashed curve, assuming a single state. Typical unreasonable J^π assignments for double-resonance fits, $J^\pi = (3/2^+, 7/2^+)$, $(5/2^+, 1/2^+)$, and $(1/2^+, 5/2^+)$ are also shown. (d) The four possible combinations are shown for two prominent resonances with $J^\pi = 3/2^+$, $5/2^+$, and $(5/2^+$ or $7/2^+)$ while the highest energy part for a bump (resonance at 2.7 MeV) was fixed by $3/2^-$. The black curve shows the fit result without the last resonance at 2.7 MeV ($J^\pi = 3/2^-$).

a better fit. Hence, we considered two resonance states, which were closely spaced, and applied several possible assignments

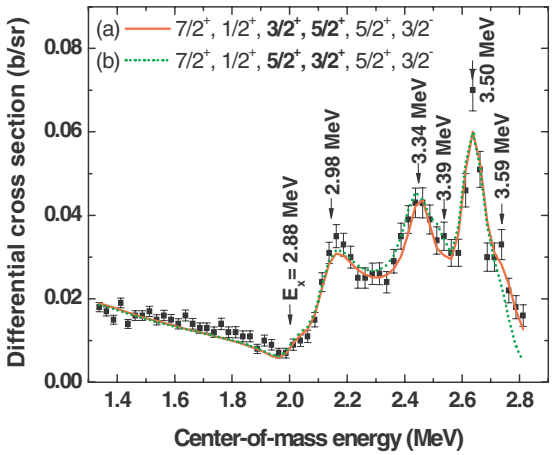

FIG. 5. (Color online) Final results as the best fits for $J^\pi = 7/2^+$, $1/2^+$, $(3/2^+, 5/2^+)$, $5/2^+$, and $3/2^-$ are shown but without firm spin-parity assignment for the doublet around 2.5 MeV.

for these two resonances when performing the R-matrix calculation. By the R-matrix analysis, is unlikely to have an assignment of $J^\pi = 1/2^+$ for one of two resonances as shown in Fig. 4(c). Moreover, although a set of J^π ($3/2^+$ and $7/2^+$) looks consistent with the data, for the $J^\pi = 7/2^+$ case, Γ_p ($\sim$66.6 keV) is much larger than the Wigner limit ($\Gamma_W = 1.0$ keV). According to the mirror nucleus, the most plausible assignments for these states are $J^\pi = 3/2^+$ and $5/2^+$, which would correspond to the doublet state of the ^{27}Mg ($E_x = 3.49$ MeV, $J^\pi = 3/2^+, 5/2^+$). A combination of $J^\pi = 3/2^+$ and $5/2^+$ was consistent with our data, but the order of $3/2^+$ and $5/2^+$ could not determined clearly because fitting results of $J^\pi = 3/2^+, 5/2^+$ and $5/2^+, 3/2^+$ did not make much of a difference [Fig. 4(d)]. Other combinations of J^π ($3/2^+$ and $3/2^+$) and ($5/2^+$ and $5/2^+$) did not yield good agreement with the data, either. Therefore, we reject these possible cases and take a combination of a $3/2^+$ and a $5/2^+$ as the J^π for a double resonance. As the spin parities of the second (around 2.48 MeV) and the last (around 2.65 MeV) prominent peaks exert influence on each other, these two peaks were calculated at the same time with two possible combinations of J^π based on comparison with the mirror ^{27}Mg nucleus and shell-model

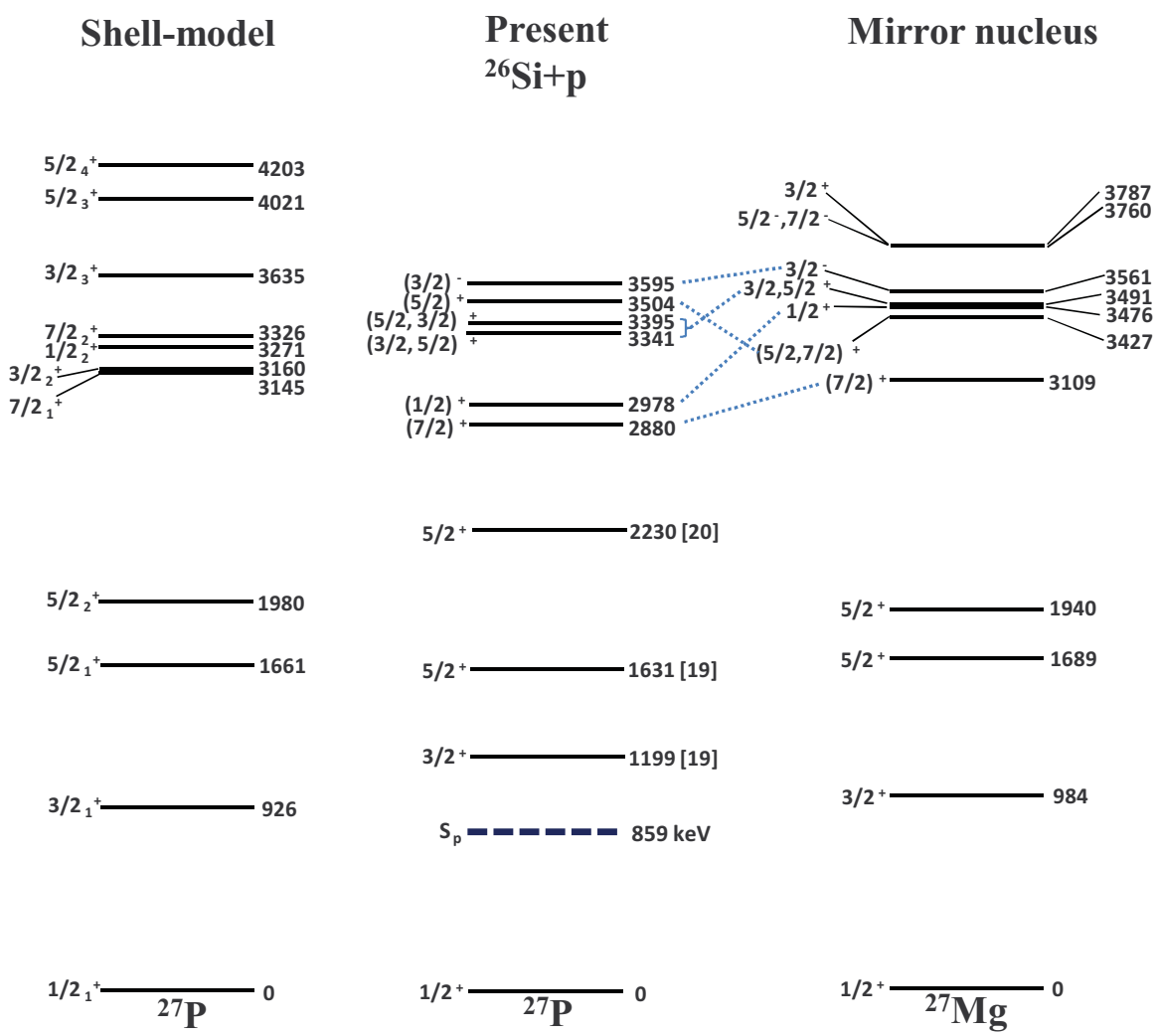

FIG. 6. Level scheme of ^{27}P obtained in present work. The shell-model calculation and the level scheme of the mirror ^{27}Mg nucleus are shown for comparison. Previously known levels [19,20] are included.

calculation. By the R-matrix analysis, most probably the 2.65 MeV state has an assignment of $J^\pi = (5/2^+$ or $7/2^+)$. In addition, this assumption is likely by comparing the level observed in the mirror nucleus [$E_x = 3.42$ MeV, $J^\pi = (5/2^+, 7/2^+)$]. The choice of $J^\pi = 7/2^+$ for the last peak can naively reproduce the data, but it would imply the existence of a resonance with a very large width ($\Gamma_p = 32.5$ keV), exceeding the Wigner limit ($\Gamma_W = 1.5$ keV). Instead, $J^\pi = 5/2^+$ was chosen for the last peak. Consequently, the R-matrix results with the combination of $J^\pi = (3/2^+, 5/2^+)$, $5/2^+$ for the resonance states at 2.48–2.65 MeV, as red (solid) and green (dotted) curves shown in Fig. 4(d), are in good accord with the experimental results.

A resonance representing a small bump around 2.74 MeV, on the right shoulder of the last peak at 2.65 MeV, was included in the R-matrix calculation. Exclusion of this bump shifted the energy of the last peak to a lower energy and resulted in a less satisfactory fit [see the black curve in Fig. 4(d)]. Thus, we introduced one resonance at this energy region, and data were fitted by using three possible spin parities, $J^\pi = 3/2^+$, $5/2^+$, and $3/2^-$, which were proposed from the comparison with the mirror ^{27}Mg nucleus. The R-matrix calculation was performed by excluding the four highest energy points because they corresponded to the highest boundary of the energy acceptance of our measurement, leading to an increased uncertainty of the R-matrix calculation. Fitting results with both $J^\pi = 3/2^+$ and $5/2^+$ for a small bump showed a deviation from the experimental data. Instead, we obtained a best fit with $J^\pi = 3/2^-$ at 3.60 MeV state. Figure 5 shows best-fit results for the excitation function of $^{26}\mathrm{Si} + p$ elastic scattering. Two spin-parity combinations are possible from our measurements for the six resonances.

The best-fit parameters are summarized in Table I. The uncertainty in energy includes both systematic and fitting uncertainty. Here the Wigner limit Γ_w was calculated by using the relation [37]

$$\Gamma_p = \frac{2\hbar^2}{M_c a_c^2} P_c C^2 S \theta_{\mathrm{sp}}^2, \tag{2}$$

TABLE I. Best-fit resonance parameters of ^{27}P obtained by the present work. The suggested possible combinations of J^π values to fit the doublet around 2.5 MeV are represented by italic letters. Spin parities for the weak resonant states at 2.02 and 2.74 MeV are put in parentheses, which means they are tentative assignments.

E_x (MeV)	$E_{c.m.}$ (MeV)	J^π	l	Γ_p (keV)	Γ_W (keV)	Previous work
2.880 (29)	2.021 (29)	$(7/2^+)$	4	5.2 ± 0.2	0.3	
2.978 (30)	2.119 (30)	$1/2^+$	0	105.4 ± 4.0	565.1	
						3.06 (9) [20]
3.341 (31)	2.482 (31)	$3/2^+, 5/2^+$	2	$31.3 \pm 1.6, 11.9 \pm 0.5$	118.0	
3.395 (31)	2.536 (31)	$5/2^+, 3/2^+$	2	$4.2 \pm 0.9, 31.2 \pm 1.9$	128.8	
						3.453 (22) [19]
3.504 (31)	2.645 (31)	$5/2^+$	2	43.4 ± 1.2	149.8	
3.595 (32)	2.736 (32)	$(3/2^-)$	1	51.0 ± 2.5	560.3	

where P_c is a penetration probability and $C^2S\theta_{sp}^2$ is the product of a spectroscopic factor C^2S and a dimensionless single-particle reduced width θ_{sp}^2. The Wigner limit can be represented for $C^2S\theta_{sp}^2 \leqslant 1$ [38]. We suggested new resonances of ^{27}P, and its parameters were extracted with improved statistics. The resonance parameters obtained in the present study all appear to be very reasonable, except for the state with $J^\pi = 7/2^+$ at 2.88 MeV, whose proton partial width exceeds the Wigner limit. This state only appears as a small bump, making it difficult to reliably determine the width for a g-wave component. Our $7/2^+$ assignment can be supported with the level scheme observed in the mirror nucleus. However, we take such a large derived width to be an artifact arising from the counting statistics for such a resonance.

C. Shell-model calculation

A new level scheme of ^{27}P deduced from the present work is shown in Fig. 6. The shell-model calculation and the level scheme of the mirror ^{27}Mg nucleus [21] are shown for comparison. Resonance states between $E_x = 2.88$ and 3.60 MeV were newly observed in the present work. The previously reported states at $E_x = 3.06$ MeV [20] and 3.453 MeV [19] lie in this excitation energy range; however, their spin parities were not clearly determined in the previous work. The shell-model calculation for the ^{27}P nucleus was performed with the shell-model code OXBASH [39] in the model space of the sd shell using WCDPN interaction [40], which contains the isovector single-particle energies, the Coulomb strength, and isovector and isotensor strengths of the nucleon-nucleon isospin-nonconserving interactions. Since ^{27}P is an odd-even nucleus with seven protons and four neutrons in the sd shell, the calculation was carried out in the sd-shell model space (SDPN) involving the $\pi 1d_{3/2}$, $\pi 1d_{5/2}$, $\pi 2s_{1/2}$, $\nu 1d_{3/2}$, $\nu 1d_{5/2}$, and $\nu 2s_{1/2}$ valence orbits. This model space allows only positive-parity states to be calculated. In addition, since ^{27}P is a sd-shell nucleus and is closed at p shell, it is difficult to produce negative-parity states by overcoming the energy gap to p shell or pf shell. Here we define the occupation ratio of the configurations of $[(\pi 1d_{5/2}^+)^6, (\pi 2s_{1/2}^+)^1, (\nu 1d_{5/2}^+)^4]$ and $[(\pi 1d_{3/2}^+)^1, (\pi 1d_{5/2}^+)^6, (\nu 1d_{5/2}^+)^4]$ to all the configurations as ρ. These two configurations are naturally produced in ^{26}Si + p scattering, because ^{26}Si at the ground state has the configuration of $[(\pi 1d_{5/2}^+)^6, (\nu 1d_{5/2}^+)^4]$. Therefore, ρ can be considered as an index which reflects the resonant strength observed in ^{26}Si + p resonant scattering. ρ for each level was calculated as in Table II. The 3.271-MeV state ($J^\pi = 1/2_2^+$) has a large $\rho = 33\%$. This state was expected to appear as a strong resonance; thus it would correspond to the first strong resonance ($E_x = 2.978$ MeV) observed in the present work. The 3.160-MeV state ($J^\pi = 3/2_2^+$) also has a large ρ of 33%, possibly corresponding to one of the observed doublet resonance ($E_x = 3.341$, 3.395 MeV). The other state in the doublet could be the 4.021 ($J^\pi = 5/2_3^+$) or 4.203 ($J^\pi = 5/2_4^+$) MeV, which have ρ of 5% and 3%, respectively. There are two $7/2^+$ states in the shell-model calculation. The 3.326-MeV state ($J^\pi = 7/2_2^+$) with 29% has relatively larger ρ than the 3.145-MeV state ($J^\pi = 7/2_1^+$) with 2%. Considering ρ, the observed state at $E_x = 2.880$ MeV is likely to be 3.326 MeV in the calculation, although the 3.145-MeV state has a closer energy. The result shows a different order of states in ^{27}P from mirror nucleus at high-lying levels as shown in the level scheme. For proton-rich nuclei, mirror symmetry breaking can be significant because of the large Coulomb shift of the orbit. ^{27}P is considered to be an example of such cases, as discussed in Ref. [41].

IV. ASTROPHYSICAL IMPLICATION

The astrophysical reaction rates of ^{26}Si$(p,\gamma)^{27}$P were previously calculated with only two resonance levels located

TABLE II. The occupation ratio of configurations of s and d waves deduced from shell-model calculations.

E_x (MeV)	J_n^π	ρ (%)
3.145	$7/2_1^+$	2
3.160	$3/2_2^+$	33
3.271	$1/2_2^+$	33
3.326	$7/2_2^+$	29
3.635	$3/2_3^+$	2
4.021	$5/2_3^+$	5
4.203	$5/2_4^+$	3

TABLE III. Relevant parameters obtained in the present work used in the reaction rate calculation.

E_x (MeV)	J^π	Total Γ_γ (eV)[a]	$\omega\gamma$ (eV)[b]
2.978	$1/2^+$	1.10×10^{-4}	1.10×10^{-4}
3.341	$3/2^+$	0.96×10^{-3}	1.92×10^{-3}
3.504	$5/2^+$	0.52×10^{-4}	1.56×10^{-4}

[a]Total $\Gamma_\gamma = \sum_{i=\text{ground,1st,2nd,3rd}} \Gamma_\gamma^i$, where $\Gamma_\gamma = \Gamma_\gamma(E2) + \Gamma_\gamma(M1)$.
[b]Since $\Gamma_p \gg \Gamma_\gamma$ in the present work, the resonance strength becomes $\omega\gamma = \omega\Gamma_\gamma = (\frac{2J+1}{2})\Gamma_\gamma$.

near the proton threshold [19,20]. We calculated the rates for the three prominent resonances clearly observed in the high-energy region above the proton threshold in the present work. The $E_x = 2.98$, 3.34, and 3.50 MeV states were assumed to have a spin parities for the case of (a) in Fig. 5. Resonant capture rates for isolated, narrow resonances are given by [19]

$$\langle \sigma v \rangle_{\text{res}} = 2.557 \times 10^{-19} (A_r T_9)^{-3/2} \omega\gamma \times \exp\left(\frac{-11.605 E_r}{T_9}\right), \quad (3)$$

where A_r is the reduced mass, T_9 is the temperature in units of GK, E_r is the resonance energy in MeV, and $\omega\gamma$ is the resonance strength. The relevant parameters were calculated and are listed in Table III.

We calculated the γ-decay width (Γ_γ) of the three prominent resonance states to the ground ($1/2^+$), first ($3/2^+$), second ($5/2^+$), and third ($5/2^+$) excited states, by $\Gamma_\gamma(E2) = \frac{B(E2)}{B^W(E2)} \Gamma_\gamma{}^W(E2)$ for the $E2$ transition and $\Gamma_\gamma(M1) = \frac{B(M1)}{B^W(M1)} \Gamma_\gamma{}^W(M1)$ for the $M1$ transition based on the Weisskopf unit. $B(E2)$ and $B(M1)$ values were calculated by the OXBASH code in the sd-shell model space using WCDPN interaction. The resulting total Γ_γ was taken as a sum of transitions to each level for the three resonances. The calculated contribution to the reaction rates are shown in Fig. 7, for each resonance obtained in this work separately along with the previous results [19], which are the direct capture and the resonant capture components. This shows the temperature dependence of the reaction rate. While the resonant capture is the dominant process for low-lying resonances to the ^{26}Si$(p,\gamma)^{27}$P rate at nova and x-ray burst temperatures, the contributions from higher-lying resonances are likely to make small but considerable impact on the reaction rate at the higher temperatures (supernovae temperatures, 10 GK). For another possible set of spin parities [case (b)], the reaction rate was calculated as the same order, and it cannot make the contribution to the reaction rates more than that of the low-lying resonances, either.

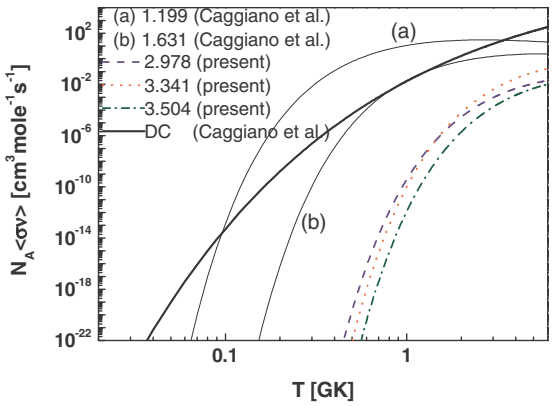

FIG. 7. The reaction rate of ^{26}Si$(p,\gamma)^{27}$P for resonances observed in the present work. The dashed and dotted curves represent the present results of the reaction rate. The solid lines are the direct capture and the resonant capture components of reaction rate estimated by Caggiano *et al.* [19] for comparison.

V. SUMMARY

We have studied the resonant elastic scattering of $^{26}\text{Si} + p$ using an RI beam at CRIB. The excitation function for the cross section of ^{27}P was measured by the thick-target method in inverse kinematics. Six resonant states in ^{27}P have been suggested, and we mostly determined their resonance parameters such as resonance energy, width, and spin parity with the R-matrix calculation. These parameters of resonant states in ^{27}P would be expected to contribute to the nuclear data as input for nuclear reaction network calculation of the rp-process nucleosysnthesis. Moreover, previous estimate of the total reaction rate of ^{26}Si$(p,\gamma)^{27}$P, which was evaluated by Iliadis *et al.* [23], should be reanalyzed with the nuclear physics input obtained in present work.

We calculated the resonant reaction rate of ^{26}Si$(p,\gamma)^{27}$P reaction up to 5 GK for the three states at $E_x = 2.98$, 3.34, and 3.50 MeV. These high-lying resonances have negligible contribution to the reaction rate at any temperature of interest. Competition between the ^{26}Si$(p,\gamma)^{27}$P reaction and ^{26}Si β decay was previously estimated in terms of density, temperature, and mass fraction of protons in stars [22]; however, the estimation was made with only two resonance levels corresponding to the first and the second excited states. It is very clear that competition between ^{26}Si(p,γ) and ^{26}Si(β^+) even when higher-lying resonant states observed in this present work are considered is unlikely to be altered significantly at higher temperatures.

ACKNOWLEDGMENTS

The experiment was performed at the RI Beam Factory operated by RIKEN Nishina Center and CNS, University of Tokyo. We are grateful to the CNS and RIKEN accelerator staff for their help. This work was supported by the National Research Foundation funded by the Korean government (NRF-2008-C00202), by the Priority Research Centers Program (2009-0093817), by the National Nuclear Research and Development Program (2010-0023862) through the National Research Foundation of Korea, by KAKEHI of Japan (Grant No. 21340053) and by the Korea-Japan Joint Research Project through NRF and JSPS.

[1] R. K. Wallace and S. E. Woosley, Astrophys. J. Suppl. **45**, 389 (1981).
[2] A. E. Champagne and M. Wiescher, Annu. Rev. Nucl. Part. Sci. **42**, 39 (1992).
[3] H. Schatz *et al*., Phys. Rev. Lett. **86**, 3471 (2001).
[4] R. Coszach *et al*., Phys. Rev. C **50**, 1695 (1994).
[5] A. Galindo-Uribarri *et al*., Nucl. Instrum. Methods B **172**, 647 (2000).
[6] T. Teranishi *et al*., Phys. Lett. B **556**, 27 (2003).
[7] H. Herndl, J. Görres, M. Wiescher, B. A. Brown, and L. VanWormer, Phys. Rev. C **52**, 1078 (1995).
[8] J. L. Fisker, H. Schatz, and F.-K. Thielemann, Astrophys. J. **174**, 261 (2008).
[9] W. A. Mahoney, J. C. Ling, A. S. Jacobson, and R. Lingenfelter, Astrophys. J. **262**, 742 (1982).
[10] N. Prantzos and R. Diehl, Phys. Rep. **267**, 1 (1996).
[11] R. Diel *et al*., Nature (London) **439**, 45 (2006).
[12] J. Knödlseder, Astrophys. J. **510**, 915 (1999).
[13] R. A. Ward and W. A. Fowler, Astrophys. J. **238**, 266 (1980).
[14] A. Coc, M.-G. Porquet, and F. Nowacki, Phys. Rev. C **61**, 015801 (1999).
[15] R. C. Runkle, A. E. Champagne, and J. Engel, Astrophys. J. **556**, 970 (2001).
[16] B. Guo, Z. H. Li, X. X. Bai, W. P. Liu, N. C. Shu, and Y. S. Chen, Phys. Rev. C **73**, 048801 (2006).
[17] N. K. Timofeyuk, P. Descouvemont, and I. J. Thompson, Phys. Rev. C **78**, 044323 (2008).
[18] W. Benenson *et al*., Phys. Rev. C **15**, 1187 (1977).
[19] J. A. Caggiano *et al*., Phys. Rev. C **64**, 025802 (2001).
[20] Y. Togano *et al*., Phys. Rev. C **84**, 035808 (2011).
[21] M. S. Basunia, Nucl. Data Sheets **112**, 1875 (2011).
[22] Y. Togano *et al*., Eur. Phys. J. A **27**, 233 (2006).
[23] C. Iliadis *et al*., Nucl. Phys. A **841**, 31 (2010).
[24] J. Y. Moon *et al*., Nucl. Phys. A **758**, 158c (2005).
[25] J. Y. Moon, Ph.D. thesis, Chung-Ang University (unpublished).
[26] S. Kubono, Y. Yanagisawa, T. Teranishi, S. Kato, Y. Kishida, S. Michimasa, Y. Ohshiro, S. Shimoura, K. Ue, S. Watanabe, and N. Yamazaki, Eur. Phys. J. A **13**, 217 (2002).
[27] Y. Yanagisawa *et al*., Nucl. Instrum. Methods Phys. Res. Sect. A **539**, 74 (2005).
[28] K. P. Artemov *et al*., Nucl. Phys. **52**, 408 (1990) [Yad. Fiz. **52**, 632 (1990)].
[29] W. Galster *et al*., Phys. Rev. C **44**, 2776 (1991).
[30] S. Kubono, Nucl. Phys. A **693**, 221 (2001).
[31] H. Yamaguchi *et al*., Nucl. Instrum. Methods Phys. Res. Sect. A **589**, 150 (2008).
[32] H. Kumagai *et al*., Nucl. Instrum. Methods Phys. Res. Sect. A **470**, 562 (2001).
[33] J. F. Ziegler, *The Stopping and Ranges of Ions in Matter*, Vols. 3 and 5 (Pergamon Press, Oxford, 1980).
[34] O. B. Tarasov and D. Bazin, Nuc. Instrum. Methods. B **266**, 4657 (2008).
[35] A. M. Lane and R. G. Thomas, Rev. Mod. Phys. **30**, 257 (1958).
[36] N. M. Larson, ORNL/TM-9179/R5, 2000 (unpublished).
[37] C. Iliadis, Nucl. Phys. A **618**, 166 (1997).
[38] T. Teichmann and E. P. Wigner, Phys. Rev. **87**, 123 (1952).
[39] B. A. Brown *et al*., MSU-NSCL Report 1289, 2005 (unpublished).
[40] W. E. Ormand and B. A. Brown, Nucl. Phys. A **491**, 1 (1989).
[41] Qi Chong *et al*., Sci. Chin. Ser. G **52**, 1464 (2009).